On the Design of Microring Resonator Devices for Switching Applications in Flexible-grid Networks

On the Design of Microring Resonator Devices for Switching Applications in Flexible-grid Networks

Jinan Xia, Andrea Bianco, Edoardo Bonetto, Roberto Gaudino
Department of Electronics and Telecommunications, Politecnico di Torino, Torino, Italy
Email: {firstname.lastname}@polito.it

***Abstract*—The physical characteristics of microring resonator switching devices are thoroughly analyzed using a model based on the field coupling matrix theory. The spectral response and insertion loss properties of these switching elements are simulated using the developed model. Results show that by cascading three microring resonators it is possible to achieve flat-top passband widths ranging from 6.25 GHz to 3 THz, while having insertion losses compatible with the use in flexible-grid optical communication networks. In light of a potential use of these devices in the design of a scalable flexible wavelength selective switch, the architecture of simple optical switches with limited functionalities is discussed.**

I. Introduction

The constant increase of traffic has urged effective use of the available spectral resources in optical core networks. The development of mature and reliable optical orthogonal frequency division multiplexing (OFDM) transmission systems helped to solve the problem. However, the adoption of optical OFDM systems made inadequate the traditional fixed-grid division of the optical spectrum used in wavelength division multiplexing (WDM) networks. Thus, in the ITU-G.694.1 recommendation the concept of flexible-grid network has been introduced. The optical spectrum is not divided according to the fixed WDM grid, but it is divided in 12.5 GHz frequency slots which can be freely used according to lightpath needs, provided that slot overlap is avoided.

In flexible-grid networks, the fundamental device is a flexible Wavelength Selective Switch (WSS) which has to cope with the need to switch channels with variable bandwidths. Early WSSs were demonstrated using integrated optics [1], [2]. Commercial WSSs use free-space optics exploiting MEMS [3] or liquid crystal switching elements [4]. Hybrid integrated and free-space optics WSSs [5] were demonstrated in laboratory. These devices cannot be used in short reach networks such as networks on chip or in board to board or data center interconnects due to their volume. The flexible-grid WSS based on AWG described in [6] requires a complex fabrication process and hardly achieves a very narrow steep-edge flat-top passband.

Microring Resonators (MRRs) are instead highly wavelength selective and can be easily integrated on chip. MRRs were studied as filters, switches, modulators, routers, multiplexers for optical communication networks and optical interconnections [7], [8]. Wide flat-top passband can be achieved by cascading several MRRs and by properly selecting structural design parameters [9], [10]. A 1.4 nm wide passband, corresponding to frequency bandwidth of 175 GHz, using three cascaded MRRs, were reported [11]. Compact 5-th order ring resonator optical filters based on submicron silicon photonic wires with flat-top pass band of 310 GHz were demonstrated [12]. A maximal bandwidth of 6 nm (750 GHz) was reported [13] . However, devices for flexible-grid networks have stricter requirements.

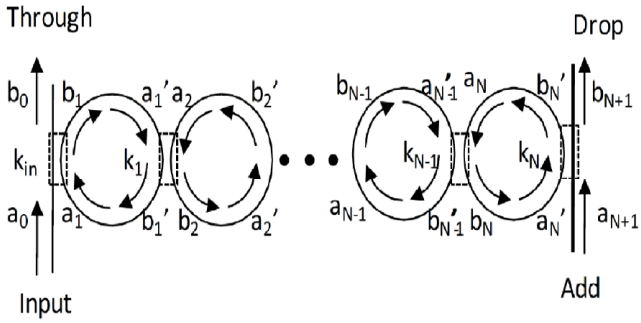

Fig. 1. Structure of a high-order MRR-based switching device.

Tuning actions are required to select a proper passband or change a passband, depending on the switching needs. Thermal [14], [15], electrical [16] or optical tuning technologies can be exploited to dynamically select a proper set of wavelengths for different switching speeds. Optimizing the design of MRRs becomes fundamental to develop MRR switching devices characterized by very narrow or very wide flat-top passband widths.

In this paper, we investigate the optimal design of high-order MRR-based devices, which are obtained by cascading several microring resonators. First, the structure and the spectral response behaviors of the MRR-based devices are illustrated in Sec. II. The spectral passband widths and insertion losses of MRR-based switching devices as a function of several physical characteristics of the MRRs, such as the coupling coefficients between MRRs, the ring diameter and the propagation losses in the MRRs are analyzed and discussed in Sec. III. In Sec. IV simple switch architectures based on MRRs are demonstrated as a possible application of the studied elements in flexible-grid networks. Finally, conclusions are drawn in Sec. V.

II. High-order Microring Resonator-based Switching Devices

High-order MRR-based devices are composed of two linear waveguides and several cascaded MRRs, as shown in Fig.1. The device cascading N microrings is named Nth-order MRR-based device. In these devices, it is assumed that all MRRs

operate at the same resonant wavelength. The signal from the input port propagates in the first waveguide. The portions of the spectrum at the resonant wavelengths are coupled into the first MRR and they propagate through the $N-1$ remaining MRRs. Finally, the propagating spectrum is coupled to the output waveguide and exits at the drop port. Instead, the portions of the spectrum not correspondent to the resonant wavelengths exit from the through port. In Fig.1, a_n, $a_n^{'}$ and b_n, $b_n^{'}$, with $n \in [0, 1, 2, ..., N]$, denote the complex mode normalized amplitudes and their squared magnitudes correspond to the modal powers. k_n represents instead the dimensionless field coupling coefficient, while k_n^2 is the power coupling coefficient.

To study the response spectrum of MRR-based devices, it is necessary to compute the resulting signal (i.e., b_{N+1}) at the drop port. The computation can be performed based on the field coupling matrix theory [17]. The light propagation in the MRR-based device can be described using the transfer matrix equation as follows:

$$\begin{bmatrix} a_{N+1} \\ b_{N+1} \end{bmatrix} = \prod_{n=0}^{N-1} (P_{N-n} \cdot Q_{N-n}) \cdot P_{in} \begin{bmatrix} a_0 \\ b_0 \end{bmatrix}. \quad (1)$$

In Eq. 1, P_n describes the coupling matrix between the $(n-1)^{th}$ and the n^{th} MRR. In particular, P_{in} and P_N correspond to the coupling matrices between the input waveguide and the first MRR, and between the output waveguide and the last MRR respectively. P_n can be computed as

$$P_n = \frac{1}{k_n} \begin{bmatrix} -t_n & 1 \\ -1 & t_n^* \end{bmatrix}, \quad (2)$$

where t_n and t_n^* are the transmission coefficient and its complex conjugate respectively. Furthermore, t_n^2 is the power coupling coefficient such that $|k_n|^2 + |t_n|^2 = 1$ with the simplifying assumption of no external losses in the coupling between bus waveguides and MRRs, and between MRRs.

Furthermore, Q_n, representing the propagation matrix in one MRR, is written as

$$Q_n = \begin{bmatrix} 0 & e^{-i\beta R\pi} \\ e^{i\beta R\pi} & 0 \end{bmatrix}, \quad (3)$$

where β is equal to $2\pi n(f)f/c + i\alpha$, $n(f)$ is the frequency dependent effective refractive index, f is the propagating mode frequency, α is the light propagation loss per unit length in the MRRs, and R is the MRR radius.

Finally, Eq. 1 can be expressed in the following form:

$$\begin{bmatrix} a_{N+1} \\ b_{N+1} \end{bmatrix} = \begin{bmatrix} A & B \\ C & D \end{bmatrix} \begin{bmatrix} a_0 \\ b_0 \end{bmatrix}, \quad (4)$$

Thus, b_0 and b_{N+1}, the signals at the through and the drop ports respectively, can be expressed as

$$b_0 = \frac{a_{N+1}}{B} - \frac{A}{B} a_0, \quad (5)$$

and

$$b_{N+1} = \frac{D}{B} a_{N+1} + \left(C - \frac{AD}{B} \right) a_0. \quad (6)$$

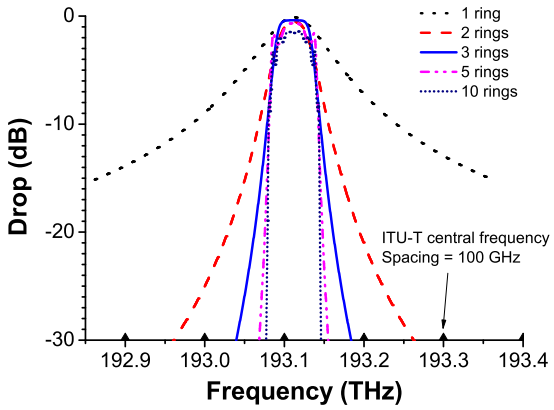

Fig. 2. Response spectrum for Nth-order MRR-based switching device for variable N, with MRR diameter $D = 20$ μm, propagation loss 3 dB/cm and power coupling coefficients $k_{in}^2 = 0.16$.

III. Physical Characterization of High-order Microring Resonator-based Switching Devices

The MRRs considered in this work are built using silicon waveguides with silicon oxide as cladding. We refer to the waveguides with cross sections of 450 nm wide and 250 nm thick, whereas the thicknesses of silicon oxide cladding at top and bottom are 1 and 3 μm respectively. The effective refractive indices of the waveguides are calculated, using the finite difference method, to be about 3.212 for transverse-electric (TE) polarization mode and 3.023 for transverse-magnetic (TM) polarization mode at the wavelength of 1.55 μm. We keep fixed these values because they depend on the waveguide structures which are the same in all the considered cases. We disregard the large wavelength shift for different polarization light propagation under resonant condition and we focus on light propagation in TE polarization only for simplicity.

The spectral response at the drop port is influenced by several physical parameters: the number of coupled MRRs, the coupling coefficients between waveguides and MRRs and between MRRs, the MRR diameter, and the propagation losses in the MRRs. In the following sections, we study the effect of each parameter on the spectral response, to determine which is the most suitable high-order MRR-based device to build WSS for flexible grid optical networks. The results are obtained by simulating the behavior of high-order MRR-based device using the mathematical formulas reported in Sec. II. In the figures, arrows are used on the frequency axis to show the ITU-T central frequency of channels with spacing 100 GHz.

All N MRRs are assumed to be identical in size. If not differently stated, the MRR diameter is set to 20 μm and the light propagation loss to 5 dB/cm. Furthermore, the power coupling coefficients between bus waveguides and MRRs are set to $k_{in}^2 = k_N^2$, and the power coupling coefficients between MRRs meet the following condition:

$$k_1^2 = k_2^2 = ... = k_{N-1}^2 = 0.25 \cdot k_{in}^4. \quad (7)$$

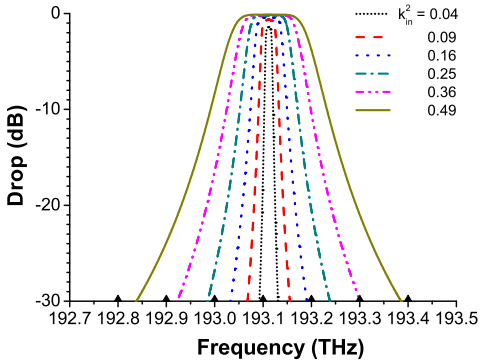

Fig. 3. Spectral response by varying k_{in}^2 the coupling coefficients between bus waveguide and MRRs, with MRR diameter $D = 20$ μm and propagation loss 3 dB/cm.

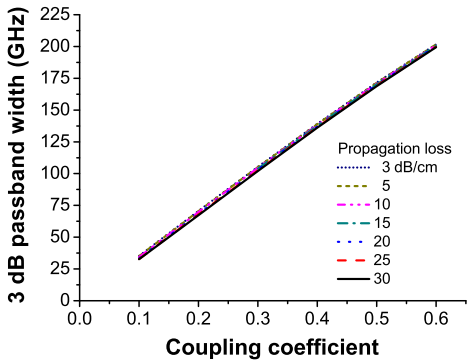

Fig. 4. 3 dB passband width as a function of coupling coefficients, with MRR diameter $D = 20$ μm.

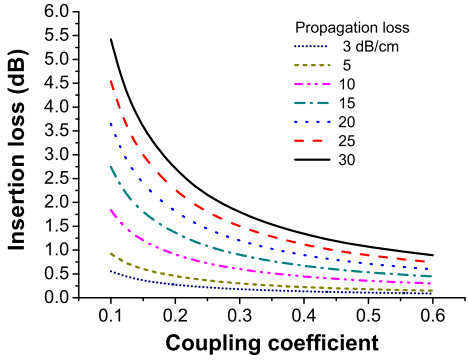

Fig. 5. Insertion loss as a function of coupling coefficients, with MRR diameter $D = 20$ μm.

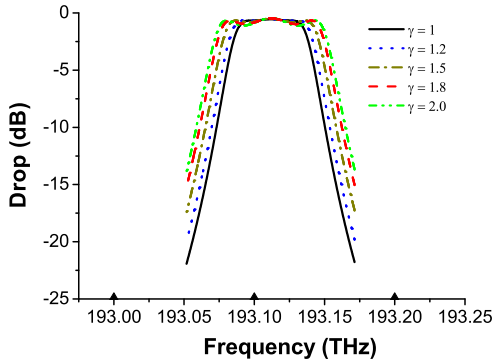

Fig. 6. 3 dB passband width as a function of the MRR 's diameter, with MRR diameter $D = 20$ μm, propagation loss 5 dB/cm and power coupling coefficients $k_{in}^2 = 0.16$.

A. Sensitivity to the Number of Microring Resonators

The desired response spectrum should present a flat-top passband to preserve signal shape and intensity. Fig. 2 depicts the response spectrum at the drop port of Nth-order MRR-based devices, for variable N, with coupling coefficients satisfying Eq. 7. A single MRR-based device has a response spectrum that corresponds to a Lorentz curve. In the case of a 2nd-order MRR-based device, the top of the response spectrum is not flat, while the coupling of three MRRs results in a flat-top passband. If more than three MRRs are used, fluctuations in the top passband appear. Thus, we focus on $N = 3$ in the following analysis, i.e., on 3rd-order MRR devices.

B. Sensitivity to power coupling coefficients and propagation losses

The spectral response of a 3rd-order MRR-based device at its drop port is analyzed by varying the coupling coefficients between MRRs, and between the bus waveguides and MRRs.

In Fig. 3 the spectral response is shown for different values of the coupling coefficients between the waveguide and the first MRR, while the coupling coefficients between the MRRs are set according to Eq. 7. The passband width increases with increasing coupling coefficients. In Fig. 4 it is shown that the 3 dB passband width of a 3rd-order MRR-based device i) increases linearly with the coupling coefficients. ii) is independent of the propagation losses ranging from 3 to 30 dB/cm. Indeed, losses almost do not affect the device passband width.

Fig. 5 reports the insertion losses, computed as the power loss between the input waveguide and the output waveguide, at the drop port of the MRR-based device as a function of the coupling coefficient with the propagation losses as a parameter. The insertion loss decreases with increasing coupling coefficients, with a steeper decrease when the power coupling coefficients are below a given threshold, between 0.2 and 0.3 depending on the propagation losses. For higher values of the power coupling coefficients the insertion loss exhibits a slower decrease. Thus, it is important to carefully adjust the value of the coupling coefficients because a small difference in coupling coefficient implies a significant change of the insertion losses. Finally, higher propagation losses imply higher values of insertion losses. Instead, for low propagation losses the insertion losses assume very low values and they are almost constant with respect to the power coupling coefficient variation.

We observed that larger flat-top passband width can be achieved if the power coupling coefficients between MRRs are increased with respect to the coupling coefficient between

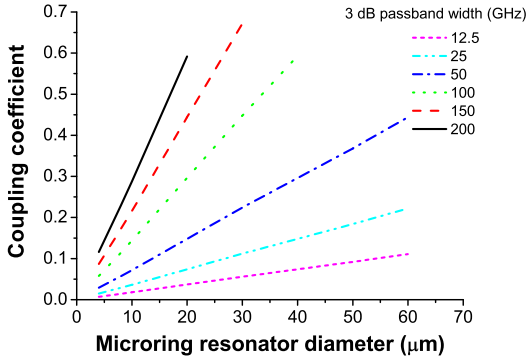

Fig. 7. 3 dB passband width as a function of the MRR 's diameter.

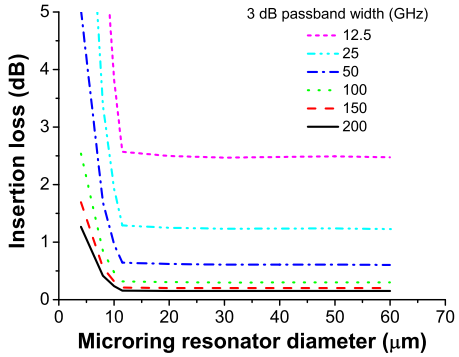

Fig. 9. Insertion loss as a function of the MRR diameter.

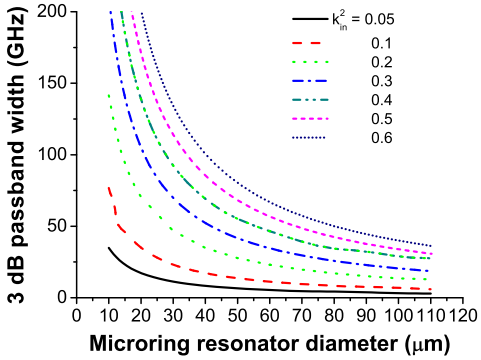

Fig. 8. 3 dB passband vs the MRR diameter, with propagation loss 5 dB/cm.

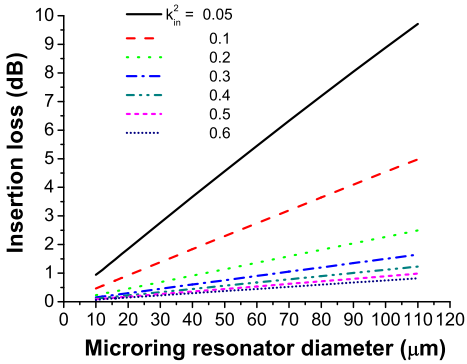

Fig. 10. Insertion loss vs MRR diameter with propagation loss 5 dB/cm.

the waveguide and the first MRR. Thus, we modify Eq. 7 by adding a coefficient γ to the equation;

$$k_1^2 = k_2^2 = 0.25 \cdot \gamma \cdot k_{in}^4, \tag{8}$$

where $\gamma \geq 1$. In Fig. 6, it is shown that the passband of the structure increases with increasing γ. If γ is larger than 1.5, the spectral response exhibits large fluctuations at the top spectrum that makes the device unsuitable for flexible grid applications.

C. Sensitivity to the ring diameter in MRR

Fig. 7 shows the coupling coefficient between the linear waveguide and the MRRs to obtain a given passband width. In the simulation, light propagation losses in the MRRs are set to 5 dB/cm when the diameters are greater than 10 μm, whereas for the diameters of 4, 8, and 10 μm, the light propagation losses in the MRRs are set to be 40, 13.1 and 7.5 dB/cm, respectively [18]. These values are exponentially dependent on the bending radii [19], [20].

To obtain a given passband bandwidth the coupling coefficients between the linear waveguides and the MRRs must be linearly increased with the MRR diameters. The coupling coefficient increase can be achieved by decreasing the gaps between the linear waveguides and MRRs.

The passband widths are instead inversely proportional to the diameters, as shown in Fig. 8, which reports the passband width as the function of MRR diameters for a light propagation losses of 5 dB/cm. The passband widths roughly decrease exponentially as the MRR diameters increase. Thus, it is better to use MRRs with small diameters to obtain large flat-top passband that can be suitable to be used in WSS based on MRRs for flexible-grid networks.

Fig. 9 shows the insertion losses as a function of the diameters of MRRs for variable passband widths. The insertion losses decrease drastically with the increase of MRR diameters until the diameters are larger than 10 μm, while for larger diameters the insertion losses are almost constant. The reason is that the bending losses increase drastically for MRRs with small diameters. In particular, the bending losses increases exponentially with the decrease in diameters when the MRR diameters are smaller than 10 μm. The insertion losses strongly depend on the bending losses for small MRRs while the propagation losses, including bending losses and intrinsic transmission losses through linear lengths become almost constants for larger MRRs.

For ring diameters larger than 10 μm the insertion losses are almost constant for a given passband width as the MRR diameters increase. Indeed, as previously described, coupling coefficients between MRRs must be increased for increasing diameters of MRRs to achieve fixed passband widths. The coupled light powers into the MRRs compensate the increased propagation losses when the MRR diameters are increased. As a result, the insertion losses of the MRR devices change very

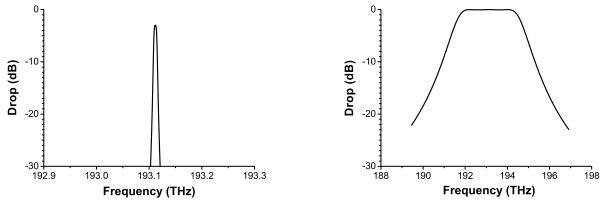

(a) 3 dB bandwidth of 6.25 GHz. (b) 3 dB bandwidth of 3 THz.

Fig. 11. Spectral response with 3 dB bandwidths of 6.25 GHz and 3 THz.

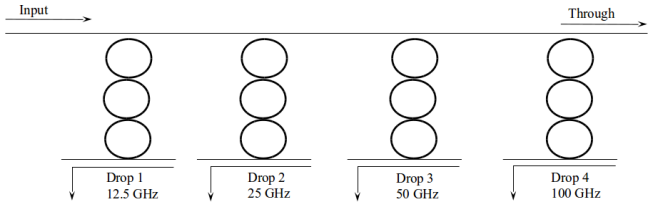

Fig. 12. Structure of a WSS with 4 drop ports at different passband widths.

little.

Finally, Fig. 10 shows the insertion loss as a function of the MRR diameters. Enlarging the MRR diameters implies not only increasing the light propagation distance in the MRRs, but also decreasing the bending loss.

IV. Applications of High-order MRR-based Switching Devices in WSS for Flexible-grid Networks

The analyzed MRR-based structures show the characteristics that can be of great benefit in designing a WSS for flexible-grid networks. Indeed, by varying the diameters or the power coupling coefficients it is possible to obtain flat-top bandwidths at the output port with highly variable, spectral responses, ranging from very narrow to very large bandwidths. For instance, Fig. 11 depicts the spectral responses with flat-top passband widths with 6.25 GHz and 3 THz bandwidths, which are respectively the minimum and the maximum passband widths that can be achieved in 3rd-order MRR-based switching devices. The narrow passband width is achieved when the MRR diameters are 20 μm, the coupling coefficient $k_{in}^2 = 0.02$, $k_1^2 = k_2^2 = 0.01$, and the propagation losses are 5 dB/cm. The wide passband width is instead achieved when the MRR diameters are 2 μm, coupling coefficients are $k_{in}^2 = 0.53$, $k_1^2 = k_2^2 = 0.2$, and propagation losses are 25 dB/cm. The insertion losses of the two elements are 4.35 dB and 0.36 dB, respectively. Thus, by properly selecting design parameters, flat-top passband with bandwidth width varying from 6.25 GHz to 3 THz using a 3rd-order MRR-based structure can be achieved. In the case that a passband wider than 3 THz is required, several MRR-based switching devices, operating at different frequencies, can be cascaded and a much wider passband can be achieved. For example, a 4 THz passband width can be achieved if we cascade two MRR-based switching devices in two continuous frequency interval having a passband width of 2 THz.

Obviously, it is required to cascade several of these devices to achieve more complex switching functionalities for a

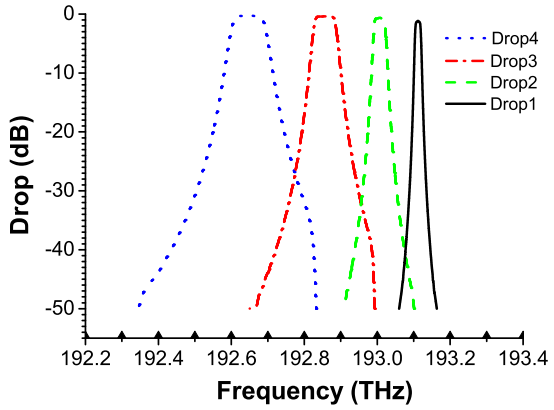

(a) Drop port

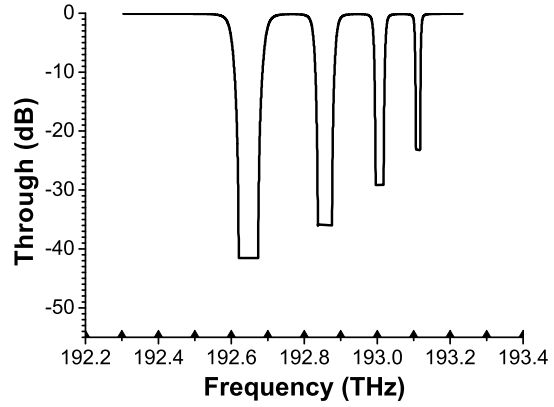

(b) Through port

Fig. 13. Transmission spectral response of WSS with 4 drop ports.

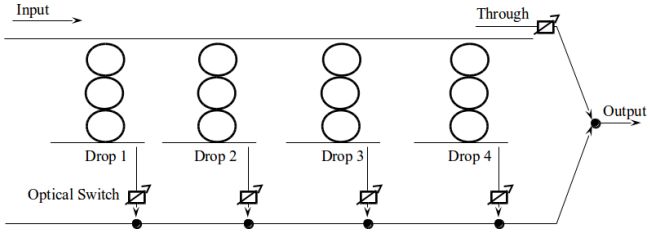

Fig. 14. Structure of a simple WSS with 4 drop ports.

flexible-grid network. A possible application for flexible-grid network is depicted in Fig.12 which represents a simple 4-stages optical switch able to switch 12.5, 25, 50, and 100 GHz 3 dB passband widths at the drop ports. In this case, all MRRs have the diameters of 20 μm with propagation loss of 5 dB/cm while coupling coefficients $k_{in}^2 = 0.037, 0.072, 0.15, 0.285$ between bus waveguides and MRRs are used. The four groups of MRRs have different effective refractive indices equal to 3.212, 3.214, 3.216, and 3.22 respectively. Fig.13 shows the transmission spectra at the four drop ports and at the through port. Insertion losses are 2.5, 1.33, 0.72 to 0.47 dB, respectively.

Another switching device which can be built with a MRR-

based structure is shown in Fig. 14. In this case MRR-based devices have the same structure and they are characterized by a 3 dB passband width of 12.5 GHz. At output ports, it is possible to select combinations of signals at the drop ports and at the through port thanks to the use of optical switches, exploiting for example Semiconductor Optical Amplifiers (SOAs). According to the required switching functionalities, the structure of Fig. 14 can be modified or it can be used as a building block for the design of a flexible WSS. The MRRs require to be properly designed (i.e., selection of the MRR diameters and of power coupling coefficients) to guarantee low losses which will ensure the scalability of the WSS. Thus, further work will consist in the study of the appropriate design of MRR-based devices to build a scalable flexible WSS.

Nevertheless, MRR devices show some limitations. The resonant wavelengths of the MRRs are sensitive to the geometrical sizes of MRRs. A very small fabrication error such as 10 nm, which reaches micro-fabrication precision limit in modern industrial processing fields, can lead to a 0.5 nm resonant wavelength shift of a MRR. Dispersion implies resonant wavelength shift and coupling coefficient variation between MRRs, the latter leading to passband widths fluctuations.

V. Conclusions

Wide flat-top passband can be achieved in 3rd-order MRR-based devices consisting of three cascaded MRRs. The passband widths of the devices are mainly influenced by the MRR diameters, the coupling coefficients between linear waveguide and MRRs, and the coupling coefficients between MRRs.

A detailed analysis on the impact of design parameters on the spectral response and on the insertion losses of these devices has been provided. The bandwidths of the devices increase linearly with the coupling coefficients while they are inversely proportional to the ring diameters. Flat-top passband width varying from 6.25 GHz to 3 THz can be achieved using 3 cascaded MRRs by properly selecting the MRR diameters and the coupling coefficients between bus waveguides and MRRs, while keeping their insertion losses acceptable.

We showed possible structures of optical switches with limited switching capabilities. Future works will investigate how scalable and full-capable switches can be built using MRR-based devices. Indeed, although in the early development stage, MRR-based switching devices seem a promising alternative to free space optics or liquid crystal switching systems which are today proposed to build WSS in the flexible-grid scenario.

Acknowledgments

The authors would like to thank Telecom Italia for their financial support in the Ph.D. grant.

References

[1] K. Okamoto, M. Okuno, A. Himeno, and Y. Ohmori, "16-channel optical add/drop multiplexer consisting of arrayed-waveguide gratings and double-gate switches," *Electronics Letters*, vol. 32, no. 16, pp. 1471–1472, 1996.

[2] C. G. P. Herben, D. H. P. Maat, X. J. M. Leijtens, M. R. Leys, Y. S. Oei, and M. Smit, "Polarization independent dilated WDM cross-connect on InP," *IEEE Photonics Technology Letters*, vol. 11, no. 12, pp. 1599–1601, 1999.

[3] J. E. Ford, V. A. Aksyuk, D. J. Bishop, and J. A. Walker, "Wavelength add-drop switching using tilting micromirrors," *Journal of Lightwave Technology*, vol. 17, no. 5, p. 904, May 1999.

[4] G. Baxter, S. Frisken, D. Abakoumov, H. Zhou, I. Clarke, A. Bartos, and S. Poole, "Highly programmable wavelength selective switch based on liquid crystal on silicon switching elements," in *Optical Fiber Communication Conference and Exposition and The National Fiber Optic Engineers Conference*, 2006, oTuF2.

[5] Y. Ishii, K. Hadama, J. Yamaguchi, Y. Kawajiri, E. Hashimoto, T. Matsuura, and F. Shimokawa, "MEMS-based 1x43 wavelength-selective switch with flat passband," in *35th European Conference on Optical Communication (ECOC)*, 2009.

[6] C. R. Doerr, L. L. Buhl, L. Chen, and N. Dupuis, "Monolithic flexible-grid 1 x 2 wavelength-selective switch in silicon photonics," *Journal of Lightwave Technology*, vol. 30, no. 4, pp. 473–478, Feb 2012.

[7] W. Bogaerts, P. D. Heyn, T. V. Vaerenbergh, K. D. Vos, S. K. Selvaraja, T. Claes, P. Dumon, P. Bienstman, D. V. Thourhout, and R. Baets, "Silicon microring resonators," *Laser & Photonics Reviews*, vol. 6, no. 1, pp. 47–73, 2012.

[8] B. G. Lee, A. Biberman, J. Chan, and K. Bergman, "High-performance modulators and switches for silicon photonic networks-on-chip," *IEEE Journal OF Selected Topics In Quantum Electronics*, vol. 16, no. 1, pp. 6–22, Jan/Feb 2010.

[9] B. E. Little, S. T. Chu, H. A. Haus, J. Foresi, and J. P. Laine, "Microring resonator channel dropping filters," *Journal Of Lightwave Technology*, vol. 15, no. 6, pp. 998–1005, Jun 1997.

[10] S. Xiao, M. H. Khan, H. Shen, and M. Qi, "Silicon-on-insulator microring add-drop filters with free spectral ranges over 30 nm," *Journal Of Lightwave Technology*, vol. 26, no. 2, pp. 228–236, Jan 2008.

[11] C. Stamatiadis, K. Vyrsokinos, L. Stampoulidis, I. Lazarou, A. Maziotis, J. Bolten, M. Karl, T. Wahlbrink, P. D. Heyn, Z. Sheng, D. V. Thourhout, and H. Avramopoulos, "Silicon-on-insulator nanowire resonators for compact and ultra-high speed all-optical wavelength converters," *Journal Of Lightwave Technology*, vol. 29, no. 20, pp. 3054–3060, Oct 2011.

[12] F. Xia, M. Rooks, L. Sekaric, and Y. Vlasov, "Ultra-compact high order ring resonator filters using submicron silicon photonic wires for onchip optical interconnects," *Optics Express*, vol. 15, no. 19, pp. 11 934–11 941, Sept 2007.

[13] L. Y. Tobing, P. Dumon, R. Baets, and M.-K. Chin, "Box-like filter response of two-dimensional array of microring resonator fabricated in silicon-on-insulator technology," in *Proceedins of 5th IEEE International Conference on Group IV Photonics*, Sorrento, Italy, Sept 2008, pp. 237–239.

[14] Y. Goebuchi, M. Hisada, T. Kato, and Y. Kokubun, "Optical cross-connect circuit using hitless wavelength selective switch," *Optics Express*, vol. 16, no. 2, pp. 535–548, Jan 2008.

[15] J. R. Ong, R. Kumar, and S. Mookherjea, "Ultra-high-contrast and tunable-bandwidth filter using cascaded high-order silicon microring filters," *IEEE Photonics Technology Letters*, vol. 25, no. 16, pp. 1543–1546, Aug 2013.

[16] X. Luo, J. Song, S. Feng, A. W. Poon, T.-Y. Liow, M. Yu, G.-Q. Lo, and D.-L. Kwong, "Silicon high-order coupled-microring-based electro-optical switches for on-chip optical interconnects," *IEEE Photonics Technology Letters*, vol. 24, no. 10, pp. 821–823, 2012.

[17] J. K. S. Poon, J. Scheuer, S. Mookherjea, G. T. Paloczi, Y. Huang, and A. Yariv, "Matrix analysis of microring coupled-resonator optical waveguides," *Optics Express*, vol. 12, no. 1, pp. 90–103, Jan 2004.

[18] S. Xiao, M. H. Khan, H. Shen, and M. Qi, "Compact silicon microring resonators with ultra-low propagation loss in the C band," *Optics Express*, vol. 15, no. 22, pp. 14 467–14 475, Oct 2007.

[19] Y. Vlasov and S. McNab, "Losses in single-mode silicon-on-insulator strip waveguides and bends," *Optics Express*, vol. 12, no. 8, pp. 1622–1631, Apr 2004.

[20] D. Marcuse, "Bend loss of slab and fiber modes computed with diffraction theory," *IEEE Journal of Quantum Electronics*, vol. 29, no. 12, pp. 2957–2961, 1993.